Nanoscale

Accepted Manuscript

This article can be cited before page numbers have been issued, to do this please use: A. Martinez-Galera and J. M. Gomez-Rodriguez, *Nanoscale*, 2025, DOI: 10.1039/D4NR04927F.

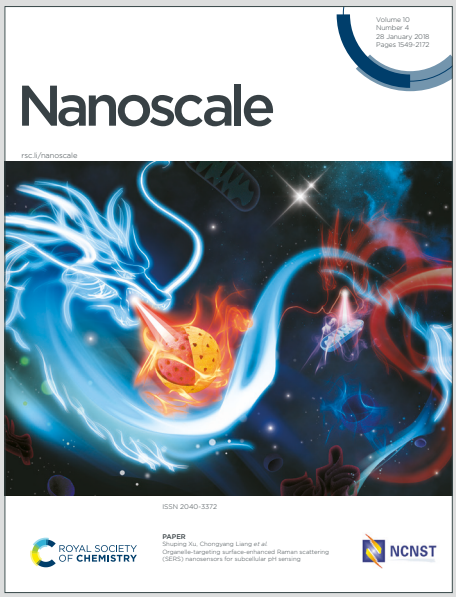

ROYAL SOCIETY OF CHEMISTRY

rsc.li/nanoscale

View Article Online
DOI: 10.1039/D4NR04927F

ARTICLE

Growing and Nanomanipulating Heterostructures of α-Bismuthene in a Nearly Isolated State

Received 00th January 20xx,
Accepted 00th January 20xx

DOI: 10.1039/x0xx00000x

Antonio J. Martínez-Galera,*[a,b,c] José M. Gómez-Rodríguez [b,c,d,] †

The growth of vertical heterostructures including bismuthene, with the lowest possible coupling to the adjacent materials, is pursued to fully exploit the exceptional properties intrinsic of the 2D allotropic forms of Bismuth. Here the growth of vertical heterostructures of ultrathin α-bismuthene and one-atom-thick h-BN layers supported on Rh(110) surfaces is reported. The scanning tunneling microscopy (STM) characterization shows that sample morphology is dominated by the presence of ultrathin a-bismuthene islands, with a lower thickness limit of two paired bilayers, randomly scattered over the h-BN surface. Unlike what has been observed in other heterostructures combining α-bismuthene with different 2D materials, which only admit specific relative angles between the atomic lattices of both constituents, any in-plane orientation of the Bi structures grown here with respect to the underlying h-BN/Rh(110) surface is possible, although certain twist angles are preferred. The larger rotational variety found in this study suggests a weaker interaction between bismuthene and h-BN, meaning that these islands could be the 2D Bi nanocrystals weaker coupled to a substrate reported till now. Additionally, pursuing an accurate control over the density, height and orientation of the islands over the h-BN/Rh(110) surface, they have been nanomanipulated by using the STM tip.

Introduction

Van der Waals heterostructures have provided a platform to observe novel physics, and currently hold high expectations facing a future implementation as building blocks in future technology [1-8]. The van der Waals epitaxy inherent to the formation of such structures allows the 2D materials in the heterostructure to retain most of their intrinsic properties, and avoids the stress associated to the lattice mismatch of conventional heteroepitaxy [9]. Atomically thin layers of Bi, for which properties as quantum size effects, Dirac cones, topological edge states, and large spin–orbit coupling have been reported, constitute a fascinating subject of study within the 2D materials family [10-13].

The most stable configurations of ultrathin Bi films are the hexagonal Bi(111) and the pseudocubic Bi(110) structures. The former, also known as β-Bismuthene [14], is characterized by a honeycomb arrangement. On the other hand, Bi(110) structure, also known as α–Bismuthene [14], can follow, either a stack of bulk truncated Bi(110) planes, or a black phosphorus (BP)-like arrangement, in which the establishment of interlayer covalent bonds by forming paired bilayers allows to saturate all dangling bonds of the two (110) planes [15]. While in the first case islands with both even and odd number of layers can be found, the latter only admits islands comprising an even number of atomic planes [16].

Previous studies of van der Waals heterostructures comprising ultrathin Bi films are scarce, and have been restricted mainly to the cases, in which they are combined with either graphene[17-19] or different 2D transition metal dichalcogenides as, for instance, $HfTe_2$[20], $TiSe_2$[21], and $NbSe_2$ [22]. In these cases Bi was arranged into the α-bismuthene structure, which was found to be oriented along specific directions of the 2D material placed below. It suggests that, although weak, the interaction between α-bismuthene and these 2D materials is sufficient to force the former to be oriented along specific angles with respect to the atomic lattice of the other constituent of the heterostructure. It opens the door to question whether it is possible to go further away by achieving heterostructures with weaker interaction between bismuthene and the other 2D material.

Despite the convenience of using an insulating support to pursue a weak interaction with other 2D materials placed on top, enabling to exploit better their intrinsic properties [23, 24], ultrathin bismuthene films have been reported mostly on conducting and semiconducting surfaces. On the other hand, it should be also taken into account that the properties of ultrathin Bi films are strongly dependent on the thickness [12, 25]. Additionally, pursuing a collective response of the heterostructures, other key factors potentially influencing the overall performance are the density of Bi islands and the possible coexistence of ones differently oriented over the

[a] Departamento de Física de Materiales, Universidad Autónoma de Madrid, Madrid E-28049, Spain
[b] Condensed Matter Physics Center (IFIMAC), Universidad Autónoma de Madrid, Madrid E-28049, Spain
[c] Instituto Nicolás Cabrera, Universidad Autónoma de Madrid, Madrid E-28049, Spain
[d] Departamento de Física de la Materia Condensada, Universidad Autónoma de Madrid, Madrid E-28049, Spain

† Deceased.

Supplementary Information available: A file with a movie is included as Supplementary material to illustrate the high precision of the nanomanipulation procedure. See DOI: 10.1039/x0xx00000x

View Article Online
DOI: 10.1039/D4NR04027F

supporting surface. Nevertheless, in all the cases mentioned above, the as-grown films were randomly scattered over the surface and exhibited different in-plane orientations and a variety of heights for a given amount of Bi. Therefore, top-down approaches allowing to avoid the coexistence of islands with different heights and in-plane orientations, as well as to control the density of islands, are required to fully exploit all the potential of these Bi based heterostructures. Here the first heterostructures comprising ultrathin bismuthene films and one-atom-thick layers of the insulating material hexagonal boron nitride (h-BN) are reported. Specifically, Bi islands exhibiting an α-bismuthene atomic arrangement have been grown under ultrahigh vacuum (UHV) conditions on h-BN/Rh(110) surfaces. This supporting surface was chosen to pursue the goal of achieving α-bismuthene layers with minimal interaction with their local environment. Thus, to ensure that the intrinsic dielectric properties of h-BN, which make this 2D material an excellent decoupling layer, are preserved to the greatest extent, it must be grown on metal surfaces giving rise to a weak interfacial coupling. In this sense, previous research has demonstrated that the symmetry mismatch between the atomic arrangements of the Rh(110) surface and 2D materials such as graphene and h-BN allows these materials to retain most of their intrinsic properties when grown on top.[26-29] The study of the rotational variety of α-bismuthene on h-BN/Rh(110) performed in this work suggests the weakest coupling found till now between bismuthene and any other 2D material. This success in the growth of nearly isolated α-bismuthene could be key for future applications, considering the intrinsic properties of this 2D material. For instance, ideal 2D alpha bismuthene exhibits robust quantum spin Hall states and a band gap linked to the bulk bands. Because of these properties, this 2D material is promising for applications in spintronics, such as long-distance spin transport and spin-to-charge conversion, as well as in topotronic devices operating efficiently at room temperature.[30] Furthermore, the as-grown islands have been accurately manipulated by using a top down approach, offering the ultimate control on their spatial distribution by means of the scanning tunneling microscope (STM) tip.

Experimental

We Experiments were performed in an UHV system, hosting a home-built STM for the atomic-scale analysis of samples. [31, 32] This experimental system is also equipped with a Low Energy Electron Diffraction (LEED) optics as a complementary tool for sample characterization.

Rh(110) single crystal surfaces were prepared by Ar^+ bombardment with an energy of the incident ions of 1keV, followed by annealing to 1200 K at an oxygen partial pressure of $2x10^{-6}$ Torr. Afterwards, the sample was further heated at 1200 K, during 300 s, and flash annealed to 1370 K. Over the so-obtained Rh(110) surfaces, h-BN monolayers were grown by chemical vapor deposition (CVD), using borazine ($B_3N_3H_6$) as precursor. Specifically, the surface of the Rh(110) supports hold at 800 C, was exposed to a borazine partial pressure of $3.5x10^{-8}$ Torr during 35 minutes. Then, Bismuthene growth was carried out by Bi sublimation from a Knudsen cell type evaporator onto the h-BN/Rh(110) samples at room temperature.

STM data were acquired and represented by using the WSxM software [33]. STM imaging was performed at the constant current mode with the bias voltage applied to the sample, while the tip was grounded.

Results and discussion

Figure 1 shows representative STM images illustrating how sample morphology varies with the amount of Bi deposited over the h-BN/Rh(110) surfaces. As observed, at low coverages Bi arranges into islands with almost regular shapes, which are found scattered over the h-BN/Rh(110) surfaces. At larger Bi coverages, the resulting islands tend to exhibit markedly elongated shapes. And finally, larger deposited amounts of Bi give rise to a network of islands, which become interconnected. Besides the geometry and spatial distribution of islands, their heights also vary with the amount of Bi deposited, with larger heights observed as the quantity of Bi increases.

The variation of sample morphology with the Bi coverage is consistent with a Volmer-Weber growth mode, which is generally associated to a larger interaction between adatoms than between them and the substrate. In turn, the nearly regular shapes of the islands suggest that Bi atoms are packed into a well-ordered structure due to cohesive interactions. This atomic packing will be further discussed along the analysis of the data summarized in Figure 2. Additionally, the in-plane orientation of the Bi arrangement with respect to the h-BN/Rh(110) surface underneath will be analyzed in Figure 3.

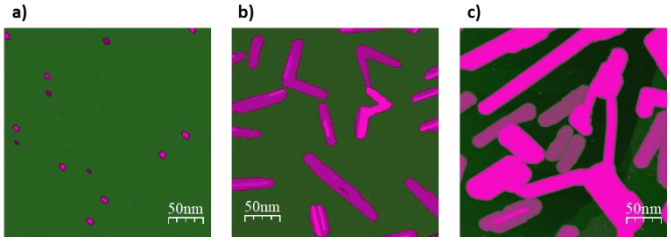

Figure 1. Spatial distribution of Bismuthene islands. **a)-c)** STM images illustrating the evolution of sample morphology with increasing the Bi coverage deposited over the h-BN/Rh(110) surfaces. The greenish hue observed in STM images is associated with the h-BN surface, while the pinkish tones correspond to islands of α-bismuthene, which have larger heights as the lighter the observed tone is. Tunneling parameters: a) V_s = +1.0 V; I_T = 0.1 nA, size: 290 × 290 nm^2; b) V_s = +1.0 V; I_T = 0.1 nA, size: 290 × 290 nm^2; c) V_s = +1.0 V; I_T = 0.1 nA, size: 290 × 290 nm^2.

Figure 2 summarizes the experimental findings about the internal structure of the islands. Specifically, Figure 2a shows an atomically resolved STM image acquired on the surface of a Bi island. A motif with rectangular geometry and lateral dimensions of 5.5 x 5.8 nm^2 is observed. This rectangular structure is also displayed in the STM topograph of Figure 2d, which was acquired around the edge of the island imaged in

View Article Online
DOI: 10.1039/D4NR04937F

Figure 2c. Concerning the vertical dimensions of the atomic packing, the apparent heights of the islands are roughly integer multiples of 0.65 nm, as shown in Figure 2b.

The existence of an ordered layout with well-defined lateral and vertical dimensions is a clear indication that the atomic arrangement proceeds according to a specific crystal structure. To interpret the information provided in Figure 2 about the atomic packing within the islands, it is convenient to keep in mind the crystal structure of bulk Bi. Specifically, Bi crystal can be understood as a rhombohedral arrangement with two atoms per unit cell [34]. The (110) plane of this structure is characterized by a rectangular lattice with lateral dimensions of 4.45x4.75 nm^2, comprising two atoms with slightly different heights along the normal to the plane [34]. Both the atomic ordering and the lateral dimensions of the Bi motif grown here are consistent with that picture, suggesting that Bi arranges over the h-BN/Rh(110) surface following a similar packing than that of (110) planes of bulk Bi. Interestingly, throughout the structural analysis conducted in this work, a domain boundary was never observed within any of the islands studied. This may indicate that the islands are single crystals.

Concerning the vertical dimensions, as above mentioned, the apparent heights of the islands are found to invariably be integer multiples of 0.65 nm, which roughly coincides with two times the separation distance between four consecutive (110) planes in bulk Bi. This fact together with the experimental findings, discussed in the preceding paragraph, constitute a clear indication that islands are composed of stacks of α-bismuthene paired bilayers, consistently with an atomic arrangement according to a BP-like structure. Accordingly, similar arrangements of Bi have been previously observed on other 2D materials as graphene [17-19], $HfTe_2$ [20], $TiSe_2$ [21], and $NbSe_2$ [22]. In these cases, the preference for the coupling into bilayers was ascribed to the establishment of interlayer bonds between undercoordinated Bi atoms, avoiding the presence of dangling bonds (see Figure 2e).

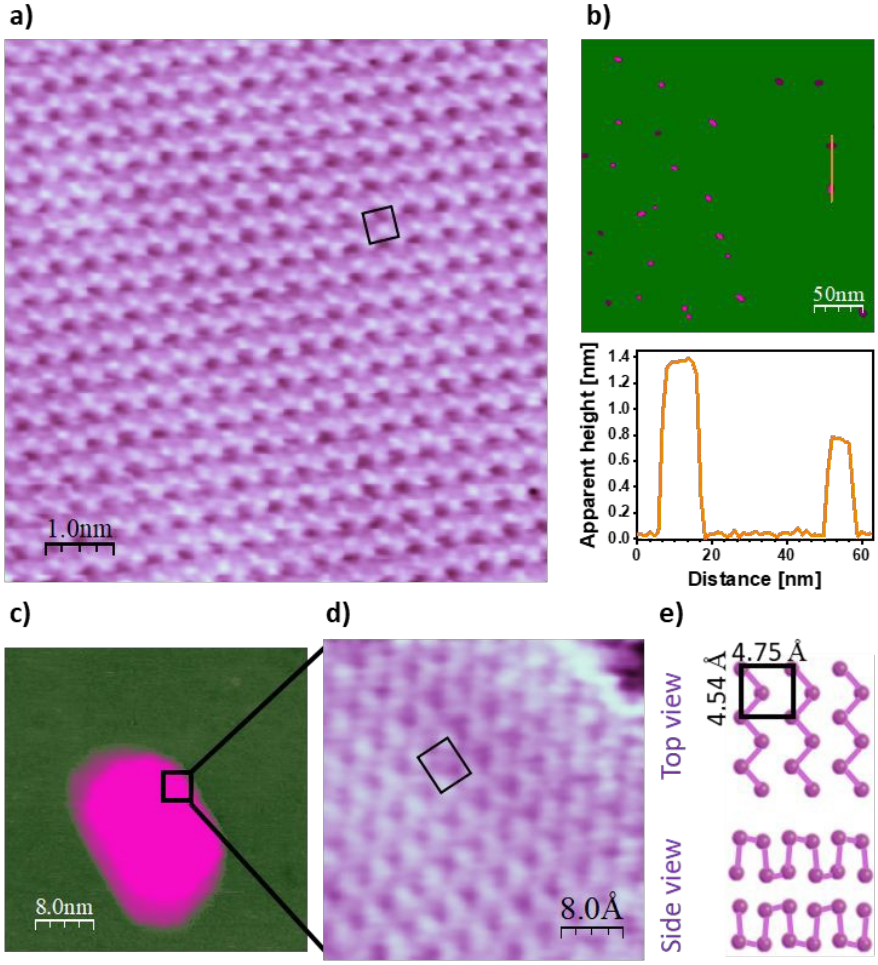

Figure 2. Internal structure of Bismuthene islands. **a)** Atomically resolved STM image displaying the atomic arrangement of Bi atoms in the surface of a Bi island; **b)** STM image displaying bismuthene islands scattered over a h-BN/Rh(110) surface (top panel), and topography profile along the orange line (bottom panel); **c)** STM image acquired over a region encompassing a Bismuthene island; **d)** Atomically resolved STM image acquired within the region indicated by the square overlaid in c), where it is observed the atomic arrangement around the island edge. **e)** Schematic representation of α-bismuthene planes stacked forming two paired bilayers The greenish hue observed in the STM images is associated with the h-BN surface, while the pinkish tones correspond to islands of α-bismuthene, which have larger heights as the lighter the observed tone is. Tunneling parameters: a) V_s = +1.21 V; I_T = 0.31 nA, size: 8 × 8 nm^2; b) V_s = +1.0 V; I_T = 0.1 nA, size: 290 × 290nm^2; c) V_s = +1.0 V; $_T$ = 0.1 nA, size: 40 × 40nm^2; d) Vs = 0.12 V; I_T = 4.53 nA, size: 4 × 4 nm^2.

View Article Online
DOI: 10.1039/D4NR04927F

Once the internal structure of the islands has been addressed, Figure 3 tackles the analysis of possible preferred relative orientations between the atomic packing of Bi and the underlying h-BN/Rh(110) surfaces. Specifically, Figure 3b shows a LEED pattern acquired on a sample with α-bismuthene islands grown over a h-BN/Rh(110) surface. As a reference to better interpret it, a LEED pattern representative of single layer h-BN grown on Rh(110) is provided in Figure 3a, where two sets of spots with hexagonal symmetry associated, respectively, to the atomic lattices of the equivalent rotational domains R-26.3 and R-33.7 are observed (see blue and red dashed arrows) [26-28]. The comparison of both patterns shows that the diffraction features arising after the growth of the α-bismuthene islands consist of a circumference and two sets of well-defined spots (see blue and red solid arrows), whose origin is discussed in the next paragraph.

A schematics providing a possible interpretation of the different diffraction features observed in the LEED patterns obtained after the growth of the α-bismuthene islands is shown in Figure 3c. According to this picture, the green circumference represents the wide rotational variety of α-bismuthene over the h-BN/Rh(110) surface. Amongst this variety, the set of spots represented by blue circumferences is associated to the orientation of the α-bismuthene unit cell with the longer side aligned, or nearly, with a zig-zag direction of the R-26.3 rotational domain of h-BN over the Rh(110) support. Accordingly, the shorter side of the unit cell must be parallel, or nearly, to the armchair direction of h-BN. Likewise, their counterpart spots represented by the red circumferences are associated to the same Bi arrangement over the R-33.7 rotational domain of the h-BN/Rh(111) surface. The existence of the circumference highlighted in green shows that any orientation between the atomic lattices of α-bismuthene and the underlying h-BN surface is found to coexist in the samples. This finding contrasts with the previously available literature reporting that α-bismuthene exhibits only specific orientations with respect to the 2D material placed underneath. For example, in the case of monolayer graphene grown on SiC, the zig-zag directions of the Bi(110) planes grown on top were found to be nearly aligned with the armchair directions of graphene.[17] Likewise, the rectangular unit cell of Bi(110) was reported to be rotated by 45° relative to the hexagonal arrangement of $HfTe_2$.[20] When grown on $TiSe_2$, the rectangular layout of Bi(110) was observed to align with the packing direction of the outermost Se atoms.[21] In the case of $NbSe_2$, a combination of STM and density functional theory (DFT) suggested an atomic arrangement in which the shorter axis of Bi(110) aligns with the zig-zag direction of $NbSe_2$.[22] The unprecedented rotational freedom of α-bismuthene found in the present work suggests that its interaction with h-BN is among the weakest reported for this 2D material in relation to its supporting surface, if not the weakest. This weak interaction is primarily attributed to van der Waals forces. It is consistent with the behavior seen in both h-BN and α-bismuthene, which are two-dimensional layered materials where the interactions between their respective atomic layers are predominantly governed by van der Waals forces.

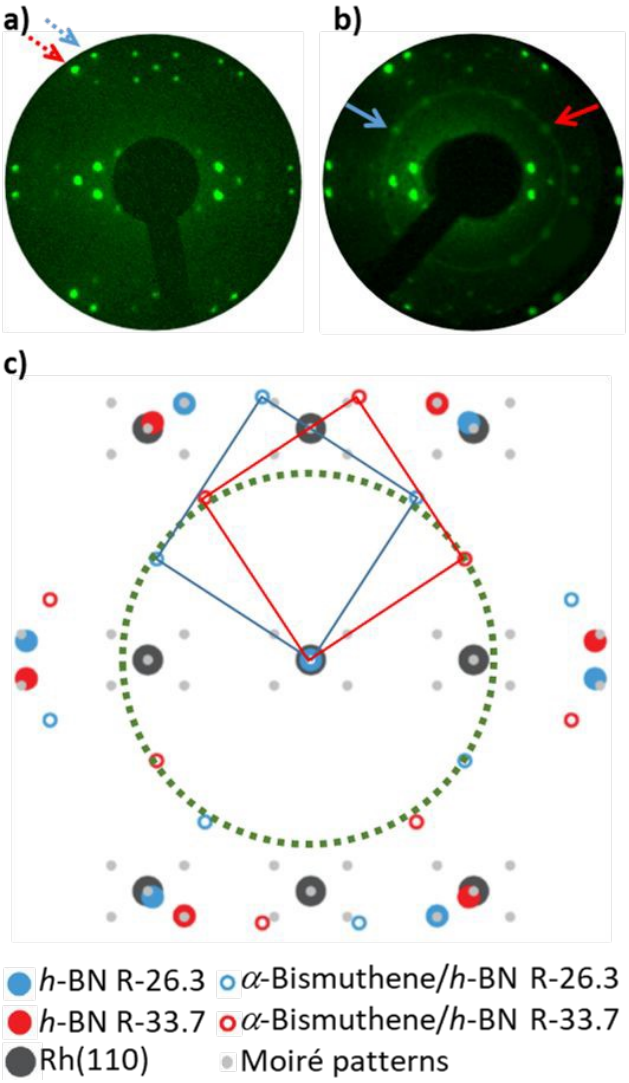

Figure 3. Relative orientation between the α-bismuthene lattice and the h-BN/Rh(110) support underneath. **a)** LEED pattern representative of the as-grown h-BN/Rh(111) surfaces; **b)** LEED pattern acquired after α-bismuthene growth on h-BN/Rh(110); **c)** schematics illustrating the origin of the different diffraction features observed in the LEED pattern shown in panel b). Electron energy a)-b) 40 eV.

As outlined in the introduction, exploiting the full potential of the exceptional properties of α-bismuthene sometimes will require to control the density and the type of the islands, pursuing a collective effect. Figure 4 displays a sequence of STM images acquired on the same region of a sample along sequential removal of the islands. To this end, after the acquisition of each image, the scan was stopped and the tip was placed over the Bi island to be removed. Afterwards, the feedback loop was opened and the tip was approached towards the selected island. After retracting back the tip, connecting

View Article Online
DOI: 10.1039/D4NR04937F

again the feedback loop, and enabling the scan over the same sample region, the selected island was no longer over the surface. As examples, Figure 4b,c show two STM images consecutively acquired after the removal of the islands highlighted in Figure 4a and 4b, respectively. Each yellow circumference indicates the island that was removed after the acquisition of the image, while the end of the arrow in the consecutive topograph points towards the empty room left behind after the removal. As observed, islands are removed regardless their high, position or orientation (see also the supplementary information for the whole sequence). Therefore, this procedure can be used to control accurately the density and the type of islands resting over the h-BN/Rh(110) surface. In line with this, as inferred from apparent heights profiles as that displayed in Figure 2b, uniform thickness in the as-grown films is not directly achievable as islands with varying heights are found to coexist over the h-BN/Rh(110) surface. Consequently, the island removal procedure could be used, for instance, as a top-down approach allowing to achieve thickness uniformity in a given region of the h-BN surface by keeping only these islands matching the desired height.

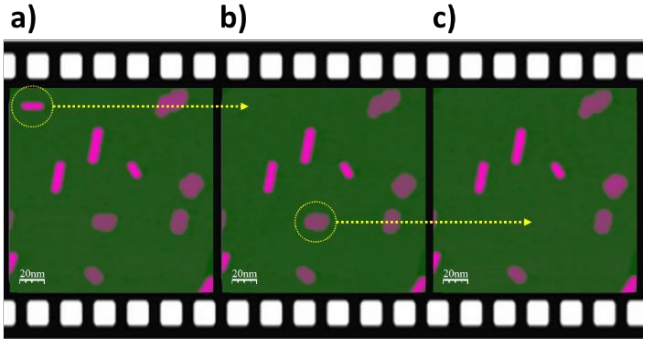

Figure 4. Nanomanipulation of α-bismuthene islands. **a)-c)** Sequence of STM images acquired after the consecutive removal of two islands. In each image, the yellow circumference highlights the island removed after stopping the scanning, while the arrow in the next topograph indicates the empty room left behind after the removal. The greenish hue observed in the STM images is associated with the h-BN surface, while the pinkish tones correspond to islands of α-bismuthene, which have larger heights as the lighter the observed tone is. Tunneling parameters: Vs = +0.39 V; I_T = 0.1. nA, size:160 × 160 nm^2 for the three images.

Conclusions

In summary, α-bismuthene islands are grown under UHV conditions on one-atom-thick h-BN resting over Rh(110) supports. Islands exhibit varying thicknesses as a function of the deposited amount of Bi with the lower limit of a paired bilayer. Atomically resolved STM images acquired over the islands show a rectangular layout with two atoms per unit cell, which is characteristic of Bi(110) planes. LEED patterns demonstrate the existence of preferred in-plane relative orientations between both constituents of the heterostructure, although they also show that every twist angle between the atomic structures of α-bismuthene and h-BN is found over the supporting Rh(110) surface. This rotational variety is unprecedented for heterostructures of α-bismuthene grown on other 2D materials. It suggests that these bismuthene islands are the ones weakest coupled to the 2D material placed underneath reported to date. By a top down approach based on nanomanipulation with the STM tip, the spatial distribution of the islands is accurately modified, allowing to select the density, size and relative orientations of the α-bismuthene-h-BN heterostructures that remain over the metal support.

Conflicts of interest

There are no conflicts to declare.

Data availability

Data are available upon request.

Acknowledgements

The authors dedicate this work to the memory of Prof. José María Gómez-Rodríguez, personal friend, mentor and colleague. Financial support from the Spanish MICINN through Projects No. PID2020-116619-GA-C22 and No. TED2021-131788A-I00, and from the Comunidad de Madrid and the Universidad Autónoma de Madrid through project SI3/PJI/2021-00500 are gratefully acknowledged.

References

1. A. K. Geim and I. V. Grigorieva, *Nature*, 2013, **499**, 419-425.
2. T. Georgiou, R. Jalil, B. D. Belle, L. Britnell, R. V. Gorbachev, S. V. Morozov, Y.-J. Kim, A. Gholinia, S. J. Haigh, O. Makarovsky, L. Eaves, L. A. Ponomarenko, A. K. Geim, K. S. Novoselov and A. Mishchenko, *Nature Nanotechnology*, 2013, **8**, 100-103.
3. X. Hong, J. Kim, S.-F. Shi, Y. Zhang, C. Jin, Y. Sun, S. Tongay, J. Wu, Y. Zhang and F. Wang, *Nature Nanotechnology*, 2014, **9**, 682-686.
4. X. Qian, J. Liu, L. Fu and J. Li, *Science*, 2014, **346**, 1344-1347.
5. D. Deng, K. S. Novoselov, Q. Fu, N. Zheng, Z. Tian and X. Bao, *Nature Nanotechnology*, 2016, **11**, 218-230.
6. Y. Liu, N. O. Weiss, X. Duan, H.-C. Cheng, Y. Huang and X. Duan, *Nature Reviews Materials*, 2016, **1**, 16042.
7. K. S. Novoselov, A. Mishchenko, A. Carvalho and A. H. Castro Neto, *Science*, 2016, **353**, aac9439.
8. Y. Cao, V. Fatemi, A. Demir, S. Fang, S. L. Tomarken, J. Y. Luo, J. D. Sanchez-Yamagishi, K. Watanabe, T. Taniguchi, E. Kaxiras, R. C. Ashoori and P. Jarillo-Herrero, *Nature*, 2018, **556**, 80-+.
9. L. A. Walsh and C. L. Hinkle, *Applied Materials Today*, 2017, **9**, 504-515.
10. H. Asahi, T. Humoto and A. Kawazu, *Phys. Rev. B*, 1974, **9**, 3347-3356.
11. Y. M. Koroteev, G. Bihlmayer, J. E. Gayone, E. V. Chulkov, S. Blügel, P. M. Echenique and P. Hofmann, *Phys. Rev. Lett.*, 2004, **93**, 046403.

View Article Online
DOI: 10.1039/D4NR04927F

12. G. Bian, X. Wang, T. Miller, T. C. Chiang, P. J. Kowalczyk, O. Mahapatra and S. A. Brown, *Phys. Rev. B*, 2014, **90**, 195409.

13. Y. Lu, W. Xu, M. Zeng, G. Yao, L. Shen, M. Yang, Z. Luo, F. Pan, K. Wu, T. Das, P. He, J. Jiang, J. Martin, Y. P. Feng, H. Lin and X.-s. Wang, *Nano Lett.*, 2015, **15**, 80-87.

14. S. Zhang, M. Xie, F. Li, Z. Yan, Y. Li, E. Kan, W. Liu, Z. Chen and H. Zeng, *Angew. Chem.-Int. Edit.*, 2016, **55**, 1666-1669.

15. K. Nagase, I. Kokubo, S. Yamazaki, K. Nakatsuji and H. Hirayama, *Phys. Rev. B*, 2018, **97,** 195418.

16. Y. M. Koroteev, G. Bihlmayer, E. V. Chulkov and S. Blügel, *Phys. Rev. B*, 2008, **77**, 045428.

17. T. Hu, X. Hui, X. Zhang, X. Liu, D. Ma, R. Wei, K. Xu and F. Ma, *Journal of Physical Chemistry Letters*, 2018, **9**, 5679-5684.

18. J. Koch, S. Sologub, C. Ghosal, T. Tschirner, A. Chatterjee, K. Pierz, H. W. Schumacher, and C. Tegenkamp. *Phys. Rev. B,* 2024, **109,** 235107.

19. J. Koch, C. Ghosal, S. Sologub and C. Tegenkamp, *J. Phys.-Condes. Matter*, 2024, **36,** 065701.

20. E. Xenogiannopoulou, D. Tsoutsou, P. Tsipas, S. Fragkos, S. Chaitoglou, N. Kelaidis and A. Dimoulas, *Nanotechnology*, 2022, **33**, 015701.

21. X. Dong, Y. Li, J. Li, X. Peng, L. Qiao, D. Chen, H. Yang, X. Xiong, Q. Wang, X. Li, J. Duan, J. Han and W. Xiao, *J. Phys. Chem. C*, 2019, **123**, 13637-13641.

22. L. Peng, J. Qiao, J.-J. Xian, Y. Pan, W. Ji, W. Zhang and Y.-S. Fu, *ACS Nano*, 2019, **13**, 1885-1892.

23. C. R. Dean, A. F. Young, I. Meric, C. Lee, L. Wang, S. Sorgenfrei, K. Watanabe, T. Taniguchi, P. Kim, K. L. Shepard and J. Hone, *Nature Nanotechnology*, 2010, **5**, 722-726.

24. Y. Cao, V. Fatemi, S. Fang, K. Watanabe, T. Taniguchi, E. Kaxiras and P. Jarillo-Herrero, *Nature*, 2018, **556**, 43-+.

25. A. K. Kundu, G. Gu and T. Valla, *ACS Applied Materials & Interfaces*, 2021, **13**, 33627-33634.

26. A. J. Martínez-Galera and J. M. Gómez-Rodríguez, *Nano Research*, 2018, **11**, 4643-4653.

27. A. J. Martínez-Galera and J. M. Gómez-Rodríguez, *Nano Research*, 2019, **12**, 1217-1218.

28. A. J. Martínez-Galera and J. M. Gómez-Rodríguez, *J. Phys. Chem. C*, 2019, **123**, 1866-1873.

29. A. J. Martínez-Galera, H. Guo, M. D. Jiménez-Sánchez, E. G. Michel, José M. Gómez-Rodríguez, *Carbon,* 2023, **205**, 294–301.

30. X. Liu , S. Zhang, S. Guo, B. Cai, S. A. Yang, F. Shan, M. Pumera and H. Zeng. *Chem. Soc. Rev.*, 2020, **49,** 263-285

31. O. Custance, S. Brochard, I. Brihuega, E. Artacho, J. M. Soler, A. M. Baró and J. M. Gómez-Rodríguez, *Phys. Rev. B*, 2003, **67**, 235410.

32. A. J. Martinez-Galera and J. M. Gomez-Rodriguez, *J. Phys. Chem. C*, 2011, **115**, 11089-11094.

33. I. Horcas, R. Fernandez, J. M. Gomez-Rodriguez, J. Colchero, J. Gomez-Herrero and A. M. Baro, *Rev. Sci. Instrum.*, 2007, **78**, 013705.

34. P. Hofmann, *Prog. Surf. Sci.*, 2006, **81**, 191-245.

View Article Online
DOI: 10.1039/D4NR04927F

Data are available upon request.